A Data-Driven Algorithm for Online Power Grid Topology Change Identification with PMUs

Shiyuan Wang, *Student Member, IEEE,* Payman Dehghanian, *Member, IEEE*, and Bei Zhang, *Member, IEEE*

***Abstract*—Power system topology change, realized either through unpredictable disturbances (faults) or transmission line switching actions in day-to-day operations, manifests itself via a number of waveforms that can be captured at the measurement points (substations) in the power grid. The waveforms acquired by the phasor measurement units (PMUs) and/or other intelligent electronic devices (IEDs) will potentially carry specific features corresponding to the event, thereby reflecting the dynamics of a network topology change. This paper proposes a novel wavelet transform algorithm, the pseudo continuous quadrature wavelet transform (PCQ-WT), for online power network topology change detection, enabling situational awareness spatially and temporally from one single PMU. Test signals representing different prevailing conditions in the grid with and without a topology change event are generated and applied to the IEEE 30-bus test system. The results verify the accurate performance of the proposed event detection and classification mechanism for online applications.**

***Index Terms*—Feature extraction; Phasor Measurement Unit (PMU); Waveform classification; Wavelet transform (WT).**

I. Introduction

The synchrophasor technology has revolutionized the traditional measurement setting in power grids into a new paradigm with high-resolution measurements. Enabling a higher situational awareness, the synchrophasosr measurements are captured across the network via phasor measurement units (PMUs). Modern power system applications, e.g., model validation, state estimation, dynamic stability monitoring, power grid real-time monitoring, protection, and control, as well as post-event analytics have been evolutionarily transformed via PMUs [1]–[5]. The operational decisions in power grid are closely dependent on its real-time topology and how the electricity flows in the network. System operators have a long history of using state estimation for supervisory control and operational planning decisions. Wide deployment of PMUs dramatically improves the topology detection process over time as the system transition into different operating states.

Waveforms in power grid typically reveal a certain pattern with specific features and peculiarities driven by the system operating conditions. For instance, phasor magnitudes and phase angles go through step changes during faults [6] and the measurements can be noisy [7]. Unbalanced load, voltage surge or sag, harmonics, and frequency drift are also common phenomena in electrical power networks. Several synchrophasor estimation algorithms (SEAs) have been proposed in the literature, the foundations of which are driven by mathematical approximations. Pattern recognition and waveform classification for power quality and fault analysis have been also researched [8]–[12]. To the best of the authors' knowledge, only a few have been focused on waveform feature extraction for online topology change detection in power grids [3], [13]. In this paper, a pseudo continuous quadrature wavelet transform (PCQ-WT) is proposed applied to the PMU input waveforms: it is dedicated to waveform feature extraction facilitating the network topology change detection and consequent waveform classification. The proposed PCQ-WT feature extraction scheme does not rely on any PMU output measurements, neither GPS timing nor SEA is needed. Meanwhile, it achieves a wide range of frequency coverage for pattern recognition— but through a reduced number of scaling factor— consequently providing more details for feature classification process with an acceptable computational burden. The performance of the proposed PCQ-WT approach has been tested and verified under various spatially and temporally categorical conditions in a test system.

In this paper, Section II presents a brief background on the waveform feature extraction and classification through continuous wavelet transform (CWT) and the pseudo-continuous wavelet transform (PCWT). Section III introduces the proposed PCQ-WT approach. Case studies are analyzed in Section IV, and the conclusions come in Section V.

II. Background and Motivation

A. Power Waveform Description

First, we define a basic representation of signals in power transmission systems. Ideally, the PMU input waveforms are time-domain sinusoidal signals, as represented in (1).

$$x_{ph}(t) = A_{ph}(t)cos\left(2\pi \int_0^t f(\tau)d\tau + \phi_{ph}(t)\right) \quad (1)$$

where $A_{ph}(t)$, $f(\tau)$, $\phi_{ph}(t)$ are, respectively, the instantaneous magnitude, fundamental frequency, and phase angles in each phase. Since the input waveform is captured from a one-phase electrical signal, $x_{ph}(t)$ is a one-dimension (1-D) waveform. During transients, there exist other frequency components in the waveform. Thus, the complete format of (1) is

$$x_{ph}(t) = \sum_{h=1}^{H} A_{ph,h}(t)cos\left(2\pi \int_0^t f_h(\tau)d\tau + \phi_{ph,h}(t)\right) \quad (2)$$

where h is the order of harmonics. During a transient state, certain combination with different values of $A_{ph,h}(t)$, $f_h(\tau)$, $\phi_{ph,h}(t)$ will appear in the three-phase power signal. An

S. Wang and P. Dehghanian are with the Department of Electrical and Computer Engineering, The George Washington University, Washington, DC 20052 USA (e-mail: shiyuan1225@gwu.edu; payman@gwu.edu).

B. Zhang is with the GEIRI North America, San Jose, CA 95134 USA (e-mail: Bei.Zhang@geirina.net).

978-1-7281-1981-6/19/$31.00 ©2019 IEEE

example is the network topology change that will affect the admittance matrix and consequently the magnitude and phase angles. This change will reveal certain features and peculiarities. Note that the admittance matrix is unique for a given network topology. Therefore, as the waveform features change when the system transition from one to another configuration, the topology change event can be detected and classified.

In both transient and steady-state conditions, power waveforms contain different frequency components. The most commonly-used multi-resolution waveform classification techniques are short-time Fourier transform (STFT) and continuous wavelet transform (CWT) [14], [15]. The Clarke transformation is first applied to convert the three-phase signal from the ABC-reference to components in stationary $\alpha\beta$-frame [16].

$$x_{\alpha\beta}(t) = x_{\alpha}(t) + jx_{\beta}(t) \tag{3}$$

$$\begin{bmatrix} x_{\alpha}(t) \\ x_{\beta}(t) \end{bmatrix} = \begin{bmatrix} \frac{2}{3} & -\frac{1}{3} & \frac{1}{3} \\ 0 & \frac{\sqrt{3}}{3} & -\frac{\sqrt{3}}{3} \end{bmatrix} \begin{bmatrix} x_A(t) \\ x_B(t) \\ x_C(t) \end{bmatrix} \tag{4}$$

Both STFT and CWT require a window (buffer) of samples to process the signal in (3) and therefore, the latency cannot be avoided. Selection of a proper window size could minimize the latency effect, but at the cost of trading off the frequency resolution. The STFT extracts the waveform frequency spectrum over time via a fixed-length moving window. In contrast, the CWT evaluates the correlations between the input signal and a preset wavelet bank consisting of a mother wavelet and its daughter wavelets. Figure 1 illustrates the feature extraction results from both STFT (a and b) and CWT (c, d, e, f) under different grid conditions. It can be clearly observed that the frequency accuracy of the STFT outperforms that of the CWT during magnitude jump conditions, but the fundamental frequency features during faults are lost. However, CWT stands out for fast feature extraction and event detection. Therefore, CWT is focused in this paper as the main waveform classification approach for online topology change detection.

B. CWT and Pseudo-CWT (PCWT)

Wavelet transform is centered on the cross-correlation computations between the signal of interest, $x_{ph}(t)$ and a designated wavelet, defined as follows:

$$X_{ph,\omega}(a,b) = \frac{1}{\sqrt{|a|}} \int_{-\infty}^{\infty} x_{ph}(t) \Psi^*(\frac{t-b}{a}) dt \tag{5}$$

where $\Psi(t)$ is the mother wavelet function and Ψ^* is the complex conjugate of $\Psi(t)$; a and b are the scaling factor and the time shift; $\Psi(\frac{t-b}{a})$ is one of the "daughter wavelets" of $\Psi(t)$ [17]. With different selections of a and b, a wavelet bank is then defined. When proper intervals for the *continuous* scaling factor along with the time shift are selected, a continuous-wavelet transform (CWT) is achieved [18]. By calculating correlation between the input signal $x(t)$ and the wavelet bank, feature matrix is the outcome.

Real-time three-phase signals are down sampled within PMUs; this continuous-time to discrete-time (C2D) sampling will, however, provide discrete signals. Sharing the same sampling rate, the wavelet loaded inside the PMU must be

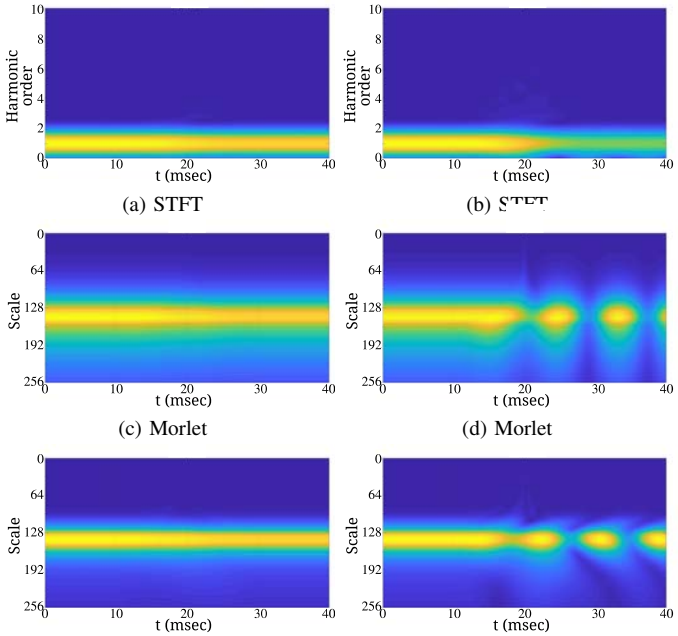

Fig. 1. Comparison of the STFT vs. Morlet CWT during: (a),(c),(e) magnitude jump events; (b),(d),(f) double-line fault events.

finite, with a wisely-selected length, thereby ensuring an acceptable latency. The CWT is pseudo continuous with finite discrete scaling factors. Here, each pseudo-CWT (PCWT) in the wavelet bank is defined as

$$X_{ph,\omega_k}(a_k,b_k) = \frac{1}{\sqrt{|a_k|}} \sum_{n=0}^{W-1} x_{ph}[n] \Psi^*[\frac{nT_s - b_k}{a_k}] \tag{6}$$

where T_s is the sampling interval; W is the window length; a_k is the k^{th} element in the vector of scaling factors with length K. The wavelet bank $\mathbf{\Psi}$ which is a $K \times W$ matrix of constant values, and the PCWT which is a $K \times 1$ matrix at each time instant n are formed as follows:

$$\mathbf{\Psi} = \begin{bmatrix} \Psi[\frac{nT_s-b_1}{a_1}] \\ \Psi[\frac{nT_s-b_2}{a_2}] \\ \vdots \\ \Psi[\frac{nT_s-b_k}{a_k}] \\ \vdots \\ \Psi[\frac{nT_s-b_K}{a_K}] \end{bmatrix}, \quad \mathbf{X}_{\omega}[n] = \begin{bmatrix} X_{\omega 1}(a_1,b_1) \\ X_{\omega 2}(a_2,b_2) \\ \vdots \\ X_{\omega k}(a_k,b_k) \\ \vdots \\ X_{\omega K}(a_K,b_K) \end{bmatrix} \tag{7}$$

The scaling factor increment is usually set to be positive; so the k^{th} daughter wavelet's central frequency is approximated:

$$f_k = F_c / a_k \tag{8}$$

where F_c is the mother wavelet's central frequency [18], which stands for the most significant frequency component.

The PCWT output needs to cover a sufficient range of frequency to provide adequate pattern information at at any given operating condition. Therefore, in addition to the fundamental frequency, the mother wavelet's central frequency F_c needs to satisfy the following condition in (9).

$$\frac{F_c}{a_K} < f_0 < F_c \tag{9}$$

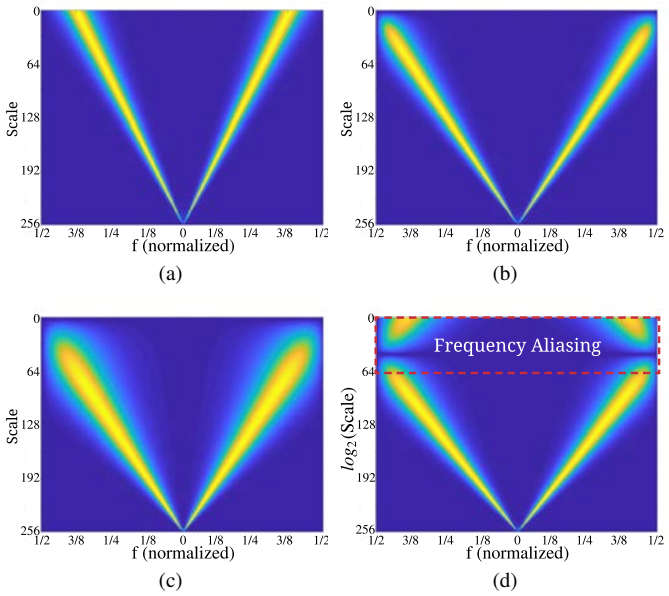

Fig. 2. Spectrum of the proposed wavelets for online feature extraction; (a) $F_c = 0.375/Ts$, $\mu = 8$ (b) $F_c = 0.5/Ts$, $\mu = 8$ (c) $F_c = 0.5/Ts$, $\mu = 4$ (d) $Fc = 0.6/Ts$, $\mu = 4$.

where f_0 is the frequency of the signal of interest. To serve the research focusing on feature extraction wavelet, F_c is chosen arbitrarily from a frequency range higher than the fundamental frequency, scaled down by a_k. Hence, as a increases, the PCWT output position decreases in the frequency domain.

III. Proposed Wavelets Based on the PCWT

A. Theoretical Foundation

The proposed wavelet performs a multi-resolution correlation calculation as described in (6). The PCWT can generally provide the frequency information through feature extraction of the power waveforms. This paper is inspired by the characteristics of narrow-bandwidth wavelets. A pass-bandwidth around the central frequency is framed: if the pass-bandwidth is wider on the high-frequency range, the high-frequency components especially appearing during transients can be easily captured and even amplified; consequently, the spectrum will show high-energy concentration in that range. In contrast, the pass-bandwidth needs to be narrow in the low-frequency range especially around the fundamental frequency, so only the fundamental frequency features can be captured. The proposed wavelet has the following format:

$$\Psi(t) = \underbrace{\frac{1/a}{cosh(2\mu\pi\frac{F_c}{a}t)}}_{\text{Vanishing Component}} \cdot \underbrace{cos(2\pi\frac{F_c}{a}t)}_{\text{Periodic Component}}. \tag{10}$$

where μ is a positive pass-bandwidth index; the larger the value of μ, the wider the pass-bandwidth will be. Equation (10) is then converted into a discrete format as follows:

$$\Psi[n] = \frac{1}{a}\frac{cos(2\pi T_s\frac{F_c}{a}n)}{cosh(2\mu\pi T_s\frac{F_c}{a}n)} \tag{11}$$

Four spectrum of the proposed wavelet bank for PCWT are demonstrated in Fig. 2. A proper value of F_c should be selected satisfying the Nyquist sampling theory; this is seen in Fig. 2 (b)-(c), where f is close to $\pm 1/2$. If F_c is larger than a threshold, aliasing occurs which will interfere the extracted features within [-1/2, -1/4] and [1/4, 1/2] in Fig. 2(d). A proper value of F_C and μ are crucial for successful feature extraction.

The PCWT process is then formulated as follows:

$$\begin{aligned} X_{\omega_k|a_k,b_k} &= \frac{1}{a_k}\sum_{n=0}^{W-1} x_{\alpha\beta}[n]\Psi^*[\frac{nT_s - b_k}{a_k}] \\ &= \frac{1}{a_k}\sum_{n=0}^{W-1}\frac{|V_{\alpha\beta}[n]|e^{j(2\pi T_s f_0 n+\theta)}cos(2\pi T_s\frac{F_c}{a_k}n)}{cosh(2\mu\pi T_s\frac{F_c}{a_k}n)} \end{aligned} \tag{12}$$

expanding (12) with all $b_k = 0$, it can be rewritten as in (13). Analytically, the window size W must have sufficient length, and thus, the first summation in (13) plays less of an impact on the energy "spectrum" than $|f_0 - \frac{F_c}{a}|$, since,

$$|f_0 + \frac{F_c}{a_k}| > |f_0 - \frac{F_c}{a_k}| \geq 0 \tag{14}$$

when $f_0 = F_c/a_k$, the PCWT will result in the highest correlation coefficients with respect to the targeted waveform.

B. Transformation of 1-D PCWT to the PCQ-WT

The time-domain $\alpha\beta$ components will be utilized to generate a complex-time signal as presented in (12) and (13). In order to ensure an effective feature extraction, the periodic component can be rewritten as a unit rotating phasor in (10), thus the proposed PCQ-WT is achieved as presented in (15).

$$\Psi[n] = \frac{1}{a_k}\frac{e^{j2\pi T_s(\frac{F_c}{a_k})n}}{cosh(2\mu\pi T_s\frac{F_c}{a_k}n)} \tag{15}$$

Therefore, equation (13) can be further simplified as in (16).

$$X_{\omega_k|a_k,0} = \frac{1}{a_k}\sum_{n=0}^{W-1}\frac{V_{\alpha\beta}[n]e^{j(2\pi T_s(f_0-\frac{F_c}{a_k})n+\theta)}}{cosh(2\mu\pi T_s\frac{F_c}{a_k}n)} \tag{16}$$

$$\begin{aligned} X_{\omega_k|a_k,0} &= \frac{1}{a_k}\sum_{n=0}^{W-1}\frac{V_{\alpha\beta}[n]e^{j(2\pi T_s f_0 n+\theta)}[e^{j(2\pi T_s\frac{F_c}{a_k}n)} + e^{-j(2\pi T_s\frac{F_c}{a_k}n)}]}{2cosh(2\mu\pi T_s\frac{F_c}{a_k}n)} \\ &= \frac{1}{a_k}\sum_{n=0}^{W-1}\frac{V_{\alpha\beta}[n]e^{j(2\pi T_s(f_0+\frac{F_c}{a_k})n+\theta)}}{2cosh(2\mu\pi T_s\frac{F_c}{a_k}n)} + \frac{1}{a_k}\sum_{n=0}^{W-1}\frac{V_{\alpha\beta}[n]e^{j(2\pi T_s(f_0-\frac{F_c}{a_k})n+\theta)}}{2cosh(2\mu\pi T_s\frac{F_c}{a_k}n)} \end{aligned} \tag{13}$$

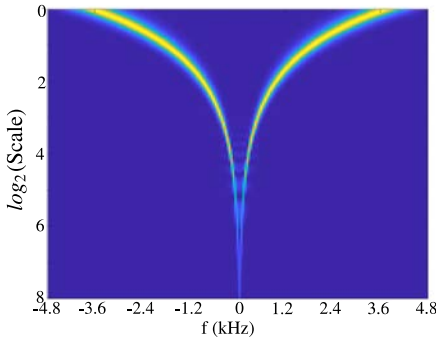

Fig. 3. Spectrum of the proposed wavelet bank, where the scaling factor is plotted by log_2.

IV. Numerical Case Studies

A. Critical Assumptions

This paper proposed a novel wavelet transform to extract and classify unique features of the input power waveforms of a PMU and correlate them with topology change events. The sampling frequency in this paper is $9600Hz$; therefore, the maximum central frequency of the proposed mother wavelet is $4800Hz$. Usually up to 50^{th} order of harmonics is considered in power system analysis; therefore, a frequency spectrum ranging from $1Hz$ to $3000Hz$—which is 0.75 times the theoretical maximum central frequency—is considered; hence, $F_c = 3000Hz$. To match the frequency spectrum, the scaling factor should ideally be [1, 3000]. However, simultaneous computation of 3000 PCWT is computationally-demanding. Therefore, conducting a down-sampling in the above frequency range is much preferred. The input signal has normally the most energy concentration in the low-frequency range, while high-frequency components will appear during transients. Hence, a dyadic scaling factor ranging $[1, 256]$, i.e., $2^{[0,8]}$, is sufficient. A total of 256 samples of exponents are uniformly selected and the scaling factor set is formed.

B. Test System and Test Cases

In order to evaluate the wavelet performance, the frequency information and patterns extracted from the input waveforms are visualized and plotted in the time domain. The IEEE 30-bus test system is selected as the test platform. The waveforms are generated from PSCAD/EMTDC using system configuration in [19] with simulation step-size of 6μs and then down-sampled to $9.6kHz$. The numerical evaluations are conducted on the following aspects: (i) waveform feature extraction during topology change in the system normal operating condition, and (ii) waveform feature extraction when a fault occurs following a topology change action. Measurements are acquired from the PMU located at Bus 6. The computation efficiency of the proposed wavelets is evaluated by measuring the time when the event occurs and that when a deformed pattern is detected. The following test cases are studied.

- *Test Case 1*: Transmission line (TL)2-4 and TL2-5 are switched-off, in two separate scenarios, when the system is in its normal operating condition.

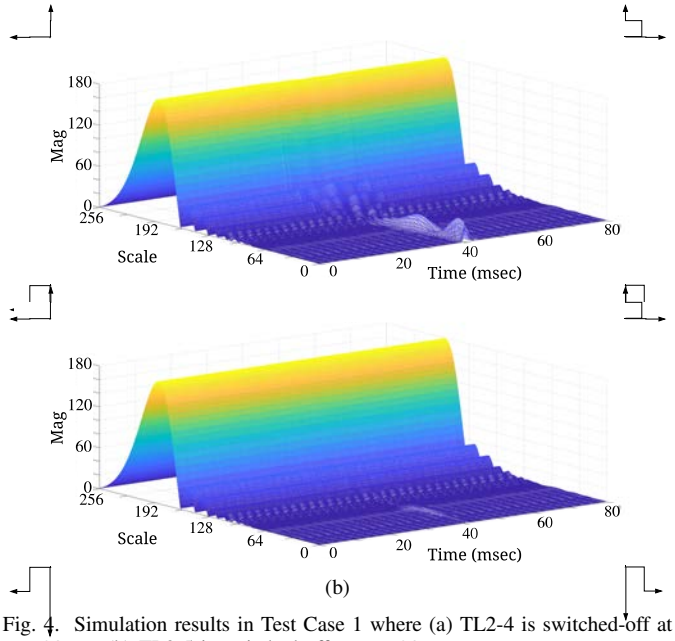

Fig. 4. Simulation results in Test Case 1 where (a) TL2-4 is switched-off at $t = 30ms$, (b) TL2-5 is switched-off at $t = 30ms$.

- *Test Case 2*: A 3-phase fault occurred at $t = 30ms$, following a topology change by disconnecting TL2-4.

C. Results and Discussions

The frequency response of the PCWT wavelet bank, used for feature extraction in the experiments, is demonstrated in Fig. 3. In Fig. 4 (a)-(b), features reveal the maximum energy concentration on the fundamental frequency. The magnitude of this energy concentration remains almost constant during both topology change practices. However, when selecting smaller scaling factors (higher frequency range), the features can be obviously differentiated. In Fig. 4, one can observe a larger energy concentration on the high-frequency range in (a) than (b). Two energy peaks are observed in 4(a), one greater than the other. In Fig. 4(b), the extracted feature corresponding to the topology change action is still obvious. It takes 10ms to reveal the significant features in both scenarios.

The Test Case 2 results are demonstrated in Fig. 5. The energy spectrum shows the fault features almost instantaneously in both Fig. 5 (a), (b). While it may be hard to visually realize the differences in Fig. 5 (a) and (b), one can see in Fig. 5 (c) that, different features are captured when two different topologies are realized, when an exact same fault appears at the same time and location (Bus 15). Based on the experiments, one may expect the possibility that different topology changes, in certain conditions, may show *similar* signatures in the data. Furthermore, the developed pattern recognition mechanism offers a promising computational performance, making it suitable for online applications.

V. Conclusion

This paper introduced a novel multi-resolution wavelet transform, i.e., the PCQ-WT, for online topology change detection and classification in power systems. The proposed approach could successfully capture unique patterns and peculiarities associated with a network topology change, either

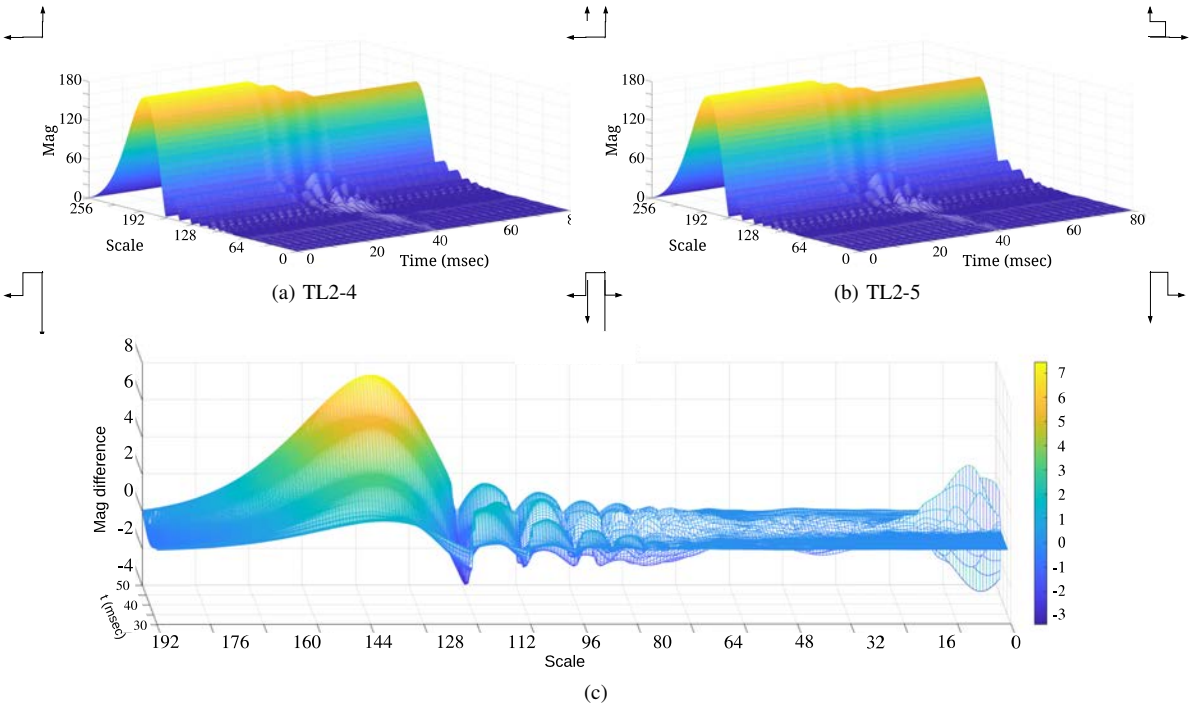

(a) TL2-4 (b) TL2-5

(c)

Fig. 5. Simulation results in Test Case 2 where 3-phase fault happens at $t = 30ms$ at Bus 15 (a) during normal operation; (b) after TL 2-4 is switched-off; (c) feature difference.

through faults or transmission topology control practices or both. The waveform classification outcome can be leveraged within PMUs, and other IEDs with PMU functionality, to archive a fast and accurate topology change detection. The performance of the proposed algorithm, in terms of feature extraction accuracy and computation time efficiency, was verified under multiple test cases representing different operating conditions in a test system.

REFERENCES

[1] E. O. Schweitzer, A. Guzmn, H. J. Altuve, D. A. Tziouvaras, and J. Needs, "Real-time synchrophasor applications in power system control and protection," in *10th IET International Conference on Developments in Power System Protection (DPSP 2010). Managing the Change*, March 2010, pp. 1–5.

[2] S. Das and T. Sidhu, "A new algorithm to compute fault synchrophasor from transient state synchrophasor in pdc," in *2013 IEEE Power Energy Society General Meeting*, July 2013, pp. 1–5.

[3] X. Liang and S. A. Wallace, "Processing synchrophasor data using a feature selection procedure," in *2016 IEEE PES Asia-Pacific Power and Energy Engineering Conference (APPEEC)*, Oct 2016, pp. 273–277.

[4] C. Thilakarathne, L. Meegahapola, and N. Fernando, "Static performance comparison of prominent synchrophasor algorithms," in *2017 IEEE Innovative Smart Grid Technologies - Asia (ISGT-Asia)*, Dec 2017, pp. 1–6.

[5] S. Das and T. Sidhu, "Robust algorithm to estimate fault synchrophasor from fault-transient synchrophasor in phasor data concentrator," *IET Generation, Transmission Distribution*, vol. 9, no. 2, pp. 124–132, 2015.

[6] F. R. Gomez, A. D. Rajapakse, U. D. Annakkage, and I. T. Fernando, "Support vector machine-based algorithm for post-fault transient stability status prediction using synchronized measurements," *IEEE Transactions on Power Systems*, vol. 26, no. 3, pp. 1474–1483, Aug 2011.

[7] J. A. de la O Serna and J. Rodrguez-Maldonado, "Taylorkalmanfourier filters for instantaneous oscillating phasor and harmonic estimates," *IEEE Transactions on Instrumentation and Measurement*, vol. 61, no. 4, pp. 941–951, April 2012.

[8] F. A. S. Borges, R. A. S. Fernandes, I. N. Silva, and C. B. S. Silva, "Feature extraction and power quality disturbances classification using smart meters signals," *IEEE Transactions on Industrial Informatics*, vol. 12, no. 2, pp. 824–833, April 2016.

[9] M. S. Manikandan, S. R. Samantaray, and I. Kamwa, "Detection and classification of power quality disturbances using sparse signal decomposition on hybrid dictionaries," *IEEE Transactions on Instrumentation and Measurement*, vol. 64, no. 1, pp. 27–38, Jan 2015.

[10] K. Thirumala, M. S. Prasad, T. Jain, and A. C. Umarikar, "Tunable-q wavelet transform and dual multiclass svm for online automatic detection of power quality disturbances," *IEEE Transactions on Smart Grid*, vol. 9, no. 4, pp. 3018–3028, July 2018.

[11] D. P. Mishra, S. R. Samantaray, and G. Joos, "A combined wavelet and data-mining based intelligent protection scheme for microgrid," *IEEE Transactions on Smart Grid*, vol. 7, no. 5, pp. 2295–2304, Sept 2016.

[12] P. Rajaraman, N. A. Sundaravaradan, R. Meyur, M. J. B. Reddy, and D. K. Mohanta, "Fault classification in transmission lines using wavelet multiresolution analysis," *IEEE Potentials*, vol. 35, no. 1, pp. 38–44, Jan 2016.

[13] C. Qian and M. Kezunovic, "A power waveform classification method for adaptive synchrophasor estimation," *IEEE Transactions on Instrumentation and Measurement*, vol. 67, no. 7, pp. 1646–1658, July 2018.

[14] C. Torrence and G. P. Compo, "A practical guide to wavelet analysis," *Bulletin of the American Meteorological society*, vol. 79, no. 1, pp. 61–78, 1998.

[15] P. S. Addison, *The illustrated wavelet transform handbook: introductory theory and applications in science, engineering, medicine and finance*. CRC press, 2017.

[16] W. Duesterhoeft, M. W. Schulz, and E. Clarke, "Determination of instantaneous currents and voltages by means of alpha, beta, and zero components," *Transactions of the American Institute of Electrical Engineers*, vol. 2, no. 70, pp. 1248–1255, 1951.

[17] M. Stephane, *A wavelet tour of signal processing*. Elsevier, 1999.

[18] S. Mallat and W. L. Hwang, "Singularity detection and processing with wavelets," *IEEE Transactions on Information Theory*, vol. 38, no. 2, pp. 617–643, March 1992.

[19] (2018, May) PSCAD IEEE 30 Bus System, Manitoba.HVDC Reserach Center. [Online]. Available: https://hvdc.ca/uploads/knowledge_base/ieee_30_bus_technical_note.pdf?t=1460659229